Rapid Communications

Critical transitions in heterogeneous networks: Loss of low-degree nodes as an early warning signal

Alessandro Loppini,[1,*] Simonetta Filippi,[1,2,*] and H. Eugene Stanley[3]

[1]*Department of Engineering, Campus Bio-Medico University of Rome, Via A. del Portillo 21, 00128 Rome, Italy*

[2]*International Center for Relativistic Astrophysics Network–ICRANet, Piazza della Repubblica 10, Pescara I-65122, Italy*

[3]*Center for Polymer Studies and Department of Physics, Boston University, Boston, Massachusetts 02215, USA*

(Received 14 November 2018; published 2 April 2019)

A large number of real networks show abrupt phase transition phenomena in response to environmental changes. In this case, cascading phenomena can induce drastic and discontinuous changes in the system state and lead to collapse. Although complex network theory has been used to investigate these drastic events, we are still unable to predict them effectively. We here analyze collapse phenomena by proposing a minimal two-state dynamic on a complex network and introducing the effect of local connectivities on the evolution of network nodes. We find that a heterogeneous system of interconnected components presents a mixed response to stress and can serve as a control indicator. In particular, before the critical transition point is reached a severe loss of low-degree nodes is observed, masked by the minimal failure of higher-degree nodes. Accordingly, we suggest that a significant reduction in less connected nodes can indicate impending global failure.

DOI: 10.1103/PhysRevE.99.040301

Many natural, economic, and social systems exhibit abrupt phase transition phenomena in response to environmental changes [1–11]. Examples include epidemic spreading, traffic networks, climatic and ecosystems changes, cell networks, and heart and brain dynamics. In this context, complex network theory has been applied to both real and humanly constructed systems and has provided useful statistical measurements and indicators able to describe such complex phenomena [12–14]. Recently a similar approach was used to investigate economic data [15]. It was found that combining a simple dynamics of internal and external failure with a reversal process of recovery in an interacting network reveals critical transitions in the percentage of active nodes and hystereses that cause the phase-flipping phenomena seen in fluctuating stock market indices. That formulation is also able to describe a more general class of processes [15].

In this contribution, we propose a generalization that takes into account network heterogeneity induced by topology, similarly to studies on epidemic spreading [16]. By using this approach, we show that the route toward the critical point is shaped by the connectivity class of the nodes, with significant consequences on the formulation of effective indicators of transition forecasting.

a. Dynamical model on networks. We consider a two-state dynamic model [15] where an "active" node can fail either because of internal factors with an intrinsic transition rate p_a or because of external influences with a rate p_s. External failures are due to factors external to the node and occur when the number of its failed neighbors exceeds a certain threshold, thus denoting a compromised functionality by a loss of feedback in interactions with other nodes. Internal failure occurs when intrinsic stresses exceed a certain level. Nodes recover at a rate p_r when they are able to mitigate destructive functional alterations. Compared to the original model [15] we introduce an equal mean recovery time from both external and internal failures and use transition rate instead of recovery time to describe the rescue process as a single transition from failed to active. We also examine heterogeneity in node connectivity. Specifically, the effective rate of a node's external failure takes into account the degree-dependent probability that it will be exposed to a fraction of failed nodes that exceeds a threshold. The threshold value depends on network degree, i.e., a damaged neighborhood must be defined locally with respect to the original local connectivity. In our model, we set this threshold at 50% of the node's original neighborhood size, based on the hypothesis that a particular node is insensitive to extrinsic failure if at least half of its neighbors are safe. Slight variations of this threshold do not alter our analysis significantly. This approach models several dynamical processes occurring in real networks, from the functional regulation of interacting cells, to epidemic and information spreading, to financial market crashes [15,17,18]. In addition, the proposed model shares similarities with the Watts model and with other generalizations analyzing cascades in networks with no intrinsic failure and recovery dynamics, and with homogeneous and normally distributed thresholds [19–21].

b. Mean-field theory. By adopting a mean-field approach it is possible to write a balance equation that regulates the dynamics of the fraction of active nodes for each degree class,

$$\frac{df_A^k(t)}{dt} = p_r\left[1 - f_A^k(t)\right] - (p_a + p_s R_k) f_A^k(t), \qquad (1)$$

where f_A^k is the fraction of active nodes in the kth class and R_k is the average probability that the neighborhood of a node of degree k is damaged. This factor takes into

*Corresponding authors: a.loppini@unicampus.it; s.filippi@unicampus.it

account the effective probability θ_k that a node of degree k connects to a failed neighbor and all the configurations in which the number of active neighbors is less than or equal to the threshold $m(k) = k/2$ (rounded down to the nearest integer), i.e., $R_k = \sum_{j=0}^{m(k)} \binom{k}{k-j} \theta_k^{k-j} (1-\theta_k)^j$, with $\theta_k = \sum_{k'} P(k'|k) f_{F_n}^{k'}$ and $f_F^k = 1 - f_A^k$. By definition, $P(k'|k)$ is the probability that a node of degree k is connected to a node of degree k'. Notably, $f_{F_n}^k$ represents the fraction of failed neighbors of degree k, i.e., the probability that a node of degree k is failed conditioned on one of its neighbors being active [20]. This is a dynamical variable satisfying Eq. (1) with $R_k = \sum_{j=0}^{m(k)-1} \binom{k-1}{k-j-1} \theta_k^{k-j-1} (1-\theta_k)^j$. Taking into account all degree classes in the network and considering both reference nodes and neighbors, Eq. (1) is a dynamical system of order $2k$. It is convenient to rewrite Eq. (1) by multiplying both sides by $1/p_a$ and by rescaling the time to be dimensionless from $\tau = p_a t$,

$$\frac{df_A^k(\tau)}{d\tau} = \tilde{p}_r \left[1 - f_A^k(\tau)\right] - (1 + \tilde{p}_s R_k) f_A^k(\tau), \qquad (2)$$

where $\tilde{p}_r = p_r/p_a$ and $\tilde{p}_s = p_s/p_a$. We investigate system behavior by analyzing steady-state active fractions of nodes for each connectivity class, by varying the dimensionless parameters $\tilde{p}_r$ and $\tilde{p}_s$, i.e., at different grades of internal and external failures occurrence, and recovery capacity. In particular, we numerically compute fixed points of Eq. (1) by slowly varying the control parameter $\tilde{p}_r$ both for positive (increments) and negative (decrements) directions at different and constant values of $\tilde{p}_s$. Fixed points calculated at $\tilde{p}_r^n$ are used as the initial guess at $\tilde{p}_r^{n+1}$. We test the behavior of the model in (i) a random network, (ii) a scale-free topology, and (iii) a spatially embedded network extracted from a finite set of nodes and shaped by nearest-neighbor interactions. We select these architectures because real networks are usually heterogeneous and exhibit features common to both random and regular networks or may show scale-free features such as hubs.

c. Random networks. We consider a Poisson degree distribution characterized by $P(k) = e^{-\langle k \rangle} \langle k \rangle^k / k!$, and by a conditional degree distribution $P(k'|k) = k' P(k')/\langle k \rangle$, peculiar of uncorrelated networks. We set the mean degree of network $\langle k \rangle = 10$ in our calculations, and restrict our analysis to $k \leqslant 25$ because this allows us to include the most significant fraction of nodes (the distribution rapidly goes to zero when $k > \langle k \rangle$). Figure 1(a) shows that at $\tilde{p}_s = 100$ the system undergoes a clear discontinuous abrupt transition and hysteresis. Note that each node subpopulation approaches the discontinuity point differently. Low-degree nodes show a smooth and strong decline in their fraction of active units. High-degree nodes remain strong until they reach the critical point. In the extreme cases of $k = 1, 2$ approximately 50%–70% of nodes are in a failed state prior to the transition point. Figures 1(b)–1(d) show that this behavior is qualitatively maintained at lower values of $\tilde{p}_s$, i.e., at lower values of the external failure rate, although the transition point shifts at lower recovery rate values. When $\tilde{p}_s = 1$ the transition is smooth for all node subpopulations. When we consider the global behavior of the ensemble, by computing the total fraction of active nodes in the network as $f_A = \sum_k P(k) f_A^k$, the differences disappear (black markers in Fig. 1). The total active fraction is discontinuous in the asymptotic solutions at high values of the spreading term and shows small variations prior to the transition, which reproduces the behavior of high-degree nodes. The partial smoothing of the global steady-state solutions as a function of the control parameter before the transition point is primarily due to the leaf ($k = 1$) and less connected nodes ($k < 6$), as was found in the local analysis. Results computed at different values of the threshold $m(k) = 2k/3, k/3$ (rounded down to the nearest integer) show that this behavior is qualitatively conserved also when nodes are more or less resistant to neighbors failure (Fig. 2), despite a shift of the transition point at lower and higher values of the spreading parameter, respectively.

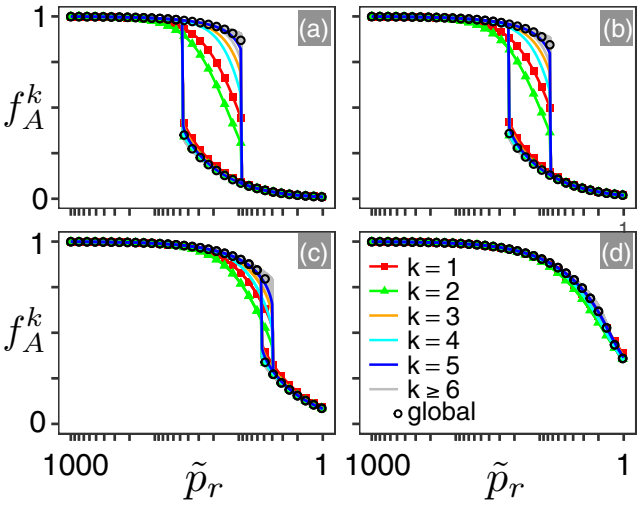

FIG. 1. Active fraction of nodes in a random uncorrelated network computed by varying the parameter $\tilde{p}_r = p_r/p_a$ at different values of $\tilde{p}_s = p_s/p_a$. (a) $\tilde{p}_s = 100$. (b) $\tilde{p}_s = 50$. (c) $\tilde{p}_s = 10$. (d) $\tilde{p}_s = 1$. Colored curves represent the active fraction of nodes for different connectivity classes of nodes. Markers represent the total active fraction of nodes in the network computed as $\sum_k P(k) f_A^k$. High values of spreading parameter show discontinuous transitions before which a significant loss of low-degree nodes can be observed.

d. Scale-free networks. We further investigate model behavior in a scale-free topology. In this case we consider a degree distribution $P(k) = k^{-\gamma}$ with $\gamma = 3$. A finite-size network of 10 000 nodes constructed with similar parameters by using the BA (Barabási-Albert) algorithm [22] showed a maximum degree of about 50. Therefore we use this cutoff in the mean-field description with the aim to keep low the dimensionality of the dynamical system and the computational cost. We also assume an uncorrelated network and adopt the same conditional degree distribution used in the random case. Active fractions of nodes in scale-free topology do not show abrupt transitions also in case of high probabilities of failures spreading [see Fig. 3(a)]. However, it is still possible to observe a larger reduction in the partial fractions of active nodes within the low-connectivity classes compared to the highly connected ones. Interestingly, in this case, these larger reductions are not masked when observing the global behavior of the network. In fact, the total fraction of active nodes mostly

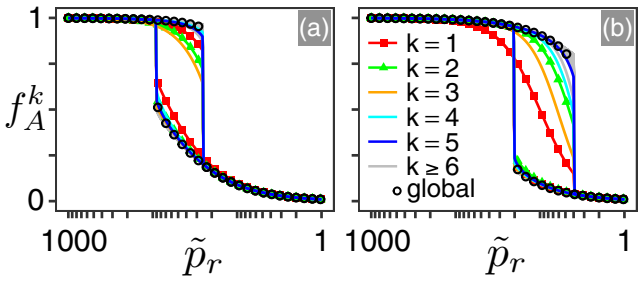

FIG. 2. Active fraction of nodes at different threshold values in a random uncorrelated network, computed by varying the parameter $\tilde{p}_r = p_r/p_a$ at $\tilde{p}_s = 100$. (a) $m(k) = 2k/3$. (b) $m(k) = k/3$. Colored curves represent the active fraction of nodes for different connectivity classes of nodes. Markers represent the total active fraction of nodes in the network computed as $\sum_k P(k) f_A^k$. The transition point in (a) and (b) occurs at lower and higher values of the spreading parameter, respectively, compared to $m(k) = k/2$, because of a lower or higher resistance of nodes to neighbors failure. In both cases, a significant loss of low-degree nodes can be observed before the abrupt transition.

represents the behavior of less connected nodes which are much more abundant than hubs in scale-free networks. Results obtained with a cutoff of $k = 100$ and $k = 200$ do not show significant differences [see Figs. 3(b) and 3(c)].

e. Spatially embedded regular networks. We finally determine model solutions in the nonrandom regular networks typical in interacting space-embedded systems in which units are physically connected. In particular, we build a spatially

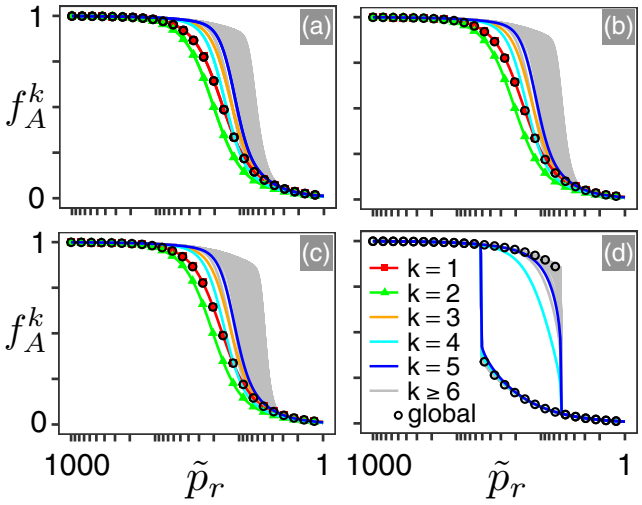

FIG. 3. Active fraction of nodes computed by varying the parameter $\tilde{p}_r = p_r/p_a$ at $\tilde{p}_s = 100$. (a) Scale-free uncorrelated network (cutoff $k = 50$). (b) Scale-free uncorrelated network (cutoff $k = 100$). (c) Scale-free uncorrelated network (cutoff $k = 200$). (d) Spatially embedded network (degree distribution and conditional degree distribution calculated from a finite-size network; see text). Colored curves represent the active fraction of nodes for different connectivity classes of nodes. Markers represent the total active fraction of nodes in the network computed as $\sum_k P(k) f_A^k$. The scale-free topology does not show abrupt transition in contrast to the spatially embedded one. Larger variations in low-degree nodes compared to high-degree nodes can be observed in both cases.

embedded network starting from a cubic lattice, fixing a three-dimensional Moore neighborhood of range 1 to set the connections. Then, we randomly remove links with $p_l = 0.3$ to induce heterogeneities. Such topological properties resemble the biological architecture of β-cell networks in endocrine pancreatic islets, an emblematic case in which communications are key in shaping emergent dynamics, cell function, and fate [23–30]. Note that this architecture can be representative of many other systems in which physical constraints shape network topology, such as highways, water distribution, and power grid networks. The resulting graph is a spatial network of $\simeq$11 000 nodes with a maximum of 26 neighbors per node. We compute statistics of the network using normalized frequency of nodes degree and normalized edge frequency between nodes of degree k and k'. Each conditional probability $P(k'|k)$ is normalized at 1. Figure 3(d) shows that prior to the transition point when the recovery rate values are decreasing, the active fraction of low-degree nodes (here $k = 4$ is the lowest degree) changes smoothly and more quickly than in high-degree nodes, in line with random and scale-free uncorrelated networks. At the transition point when the network globally collapses, the active fraction of all node classes becomes discontinuous. In line with the random network, the total fraction of active nodes is representative of the high-degree nodes of the network, while the larger reductions in the active fraction of lower degree nodes are masked.

f. Validation of mean-field analysis. To check whether mean-field theory correctly describes real networks behavior, we further simulated the two-state dynamical model in three finite-size networks of 10 000 nodes (11 056 for the spatially embedded case) characterized by the three topologies discussed above. In this case, the stochastic nature of the process is not smoothed by the thermodynamic limit. In particular, numerical simulations are performed via random evolutions of the networks by using a Monte Carlo method. All nodes are initialized in an active or failed state depending on the initial value of the parameter $\tilde{p}_r$ and on the direction of variation: failed state for low $\tilde{p}_r$ and increments of the parameter, active state for high $\tilde{p}_r$ and decrements of the parameter. To compute steady-state average fractions of nodes we adiabatically changed the control parameter and calculated the time-averaged numbers of active nodes within each connectivity class at every step, discarding a proper initial period to avoid the effect of transient responses on steady-state estimates. We then used the final state of the network to set the initial state at the next $\tilde{p}_r$ value. Numerical simulations confirmed the results obtained with the mean-field analysis (Fig. 4). When varying the control parameter, the active fractions of nodes show fluctuations around a smoothly varying mean value that follows the mean-field solutions for all the connectivity classes. Although the critical point is slightly shifted at lower values of the control parameter, the emergent phenomena are qualitatively unchanged.

Our results show that adding heterogeneity to the mathematical representation of a dynamical network produces a qualitatively different response from each connectivity class of nodes. The leaf and less connected nodes display an emergent behavior similar to that in sparse topologies, and highly clustered nodes display abrupt transitions in their active

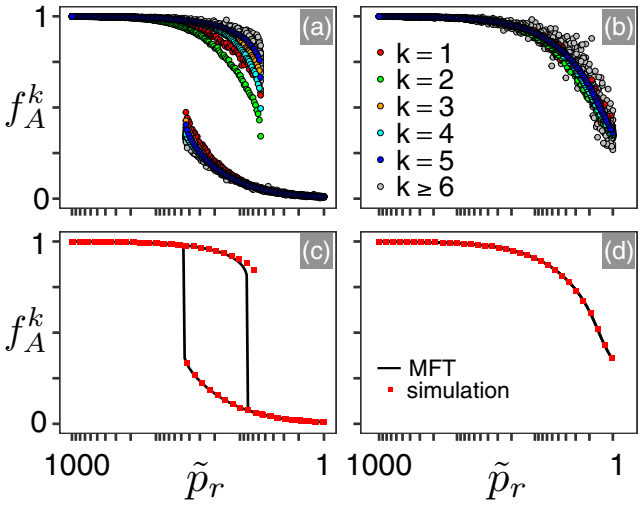

FIG. 4. Active fraction of nodes numerically computed in a finite-size ($N = 10\,000$) random uncorrelated network computed by varying the parameter $\tilde{p}_r = p_r/p_a$ at different values of $\tilde{p}_s = p_s/p_a$. (a) $\tilde{p}_s = 100$. (b) $\tilde{p}_s = 1$. (c) Comparison of global behavior between numerical simulations and mean field at $\tilde{p}_s = 100$. (d) Comparison of global behavior between numerical simulations and mean field at $\tilde{p}_s = 1$. Colored points in (a) and (b) denote the active fraction of nodes for different classes of nodes. Black curves and red squares in (c) and (d) represent the total active fraction of nodes in the network for mean field and simulations, respectively, computed as $\sum_k P(k) f_A^k$.

fraction that resemble the global behavior of strongly connected networks responding to changes in control parameters. This is in line with the increased failure probability of low-degree nodes in small cascade regimes and with hysteresis observed in similar threshold models [20,21]. However, these formulations do not include recovery and intrinsic failure and are based on different threshold rules. Our results are also similar to the original Watts model [19] in the case of large extrinsic failure probability, where threshold has significant effects. It is worth mentioning that, in our case, fixing the threshold to $k/2$ rounded down induces asymmetry between even and odd degrees in the partial active fraction of nodes. In particular, our choice makes odd degree nodes to be susceptible to external failure at more than 50% of failed neighbors. Instead, even nodes became susceptible exactly at 50% of failed neighbors and, thus, are more likely to fail. The asymmetry changes by setting the threshold to $k/3$ or $2k/3$, and this is again mostly linked to the percentage of neighbors which have to be failed to make the node susceptible. Notably, while in scale-free networks the global fraction of active nodes is strongly representative of less connected nodes, in random and spatially embedded networks the opposite holds, and large reductions in less connected nodes are masked in the global response. In these specific cases, relying on a global indicator of network functionality, such as the total fraction of active nodes, is likely to be misleading and can significantly underestimate failure risk and the probability of critical collapses. Indicators of catastrophic transitions based on slowing down of the recovery dynamics from perturbations and flickering phenomena in the state of the system have been proposed in the literature [31,32]. In particular, they were applied to the identification of catastrophic changes in climate, ecologic mutualistic communities, and depression development [33–35]. These dynamical indicators have a different nature compared to the steady states here analyzed, which instead are not dynamical by definition. However, they are strictly linked to critical bifurcation points and bistability of the dynamical system and, thus, to the underlying steady solutions on which we based our analysis. Here we suggest that monitoring loss in leaf and less connected nodes in networks showing critical discontinuous transitions gives additional perspectives on catastrophic failure prediction. Moreover, if the intrinsic dynamics of the network is considerably faster than the characteristic time which rules stressful parameters variation, time-window measures of the average active fraction on nodes based on their connectivity class have the potential to be adopted in a dynamical perspective. Future investigations will be devoted to a detailed time analysis using predictive indicators based on the observed phenomena, as well as testing the effects of other threshold rules and nodes correlation [36,37].

In conclusion, our results reveal that losing leaf and less connected nodes in response to stress may be a general feature of complex systems characterized by dynamical units whose behavior is regulated in heterogeneous complex networks. Based on the very general dynamics used to model nodes evolution, we believe that the observed behavior has potential impacts on understanding the response of several natural and artificial systems upon degradation, and it will encourage expanded research investigating such possibility in real scenarios.

Acknowledgments. A.L. and S.F. acknowledge support from the International Center for Relativistic Astrophysics Network (ICRANet) and Gruppo Nazionale per la Fisica Matematica (GNFM-INdAM). The Boston University Center for Polymer Studies is supported by NSF Grant PHY-1505000 and by DTRA Grant HDTRA1-14-1-0017.

[1] V. Colizza, R. Pastor-Satorras, and A. Vespignani, Nat. Phys. **3**, 276 (2007).
[2] W. Wang, M. Tang, H. E. Stanley, and L. A. Braunstein, Rep. Prog. Phys. **80**, 036603 (2017).
[3] Q.-H. Liu, L.-F. Zhong, W. Wang, T. Zhou, and H. Eugene Stanley, Chaos **28**, 013120 (2018).
[4] Z. Su, W. Wang, L. Li, J. Xiao, and H. E. Stanley, Sci. Rep. **7**, 6103 (2017).
[5] K. Kiyono, Z. R. Struzik, and Y. Yamamoto, Phys. Rev. Lett. **96**, 068701 (2006).
[6] T. M. Lenton, H. Held, E. Kriegler, J. W. Hall, W. Lucht, S. Rahmstorf, and H. J. Schellnhuber, Proc. Natl. Acad. Sci. USA **105**, 1786 (2008).
[7] T. Nagatani, Rep. Prog. Phys. **65**, 1331 (2002).
[8] D. Li, B. Fu, Y. Wang, G. Lu, Y. Berezin, H. E. Stanley, and S. Havlin, Proc. Natl. Acad. Sci. USA **112**, 669 (2015).
[9] K. Kiyono, Z. R. Struzik, N. Aoyagi, F. Togo, and Y. Yamamoto, Phys. Rev. Lett. **95**, 058101 (2005).

[10] H. Stanley, L. Amaral, S. V. Buldyrev, P. Gopikrishnan, V. Plerou, and M. Salinger, Proc. Natl. Acad. Sci. USA **99**, 2561 (2002).
[11] F. Morone, K. Roth, B. Min, H. E. Stanley, and H. A. Makse, Proc. Natl. Acad. Sci. USA **114**, 3849 (2017).
[12] R. Albert and A.-L. Barabási, Rev. Mod. Phys. **74**, 47 (2002).
[13] S. N. Dorogovtsev, A. V. Goltsev, and J. F. F. Mendes, Rev. Mod. Phys. **80**, 1275 (2008).
[14] A. Giuliani, S. Filippi, and M. Bertolaso, Front. Genet. **5**, 83 (2014).
[15] A. Majdandzic, B. Podobnik, S. V. Buldyrev, D. Y. Kenett, S. Havlin, and H. E. Stanley, Nat. Phys. **10**, 34 (2014).
[16] R. Pastor-Satorras and A. Vespignani, Phys. Rev. E **65**, 035108(R) (2002).
[17] J. E. Trosko, J. Cell Commun. Signal. **5**, 53 (2011).
[18] R. Pastor-Satorras, C. Castellano, P. Van Mieghem, and A. Vespignani, Rev. Mod. Phys. **87**, 925 (2015).
[19] D. J. Watts, Proc. Natl. Acad. Sci. USA **99**, 5766 (2002).
[20] J. P. Gleeson and D. J. Cahalane, Phys. Rev. E **75**, 056103 (2007).
[21] R. Burkholz, A. Garas, and F. Schweitzer, Phys. Rev. E **93**, 042313 (2016).
[22] A.-L. Barabási and R. Albert, Science **286**, 509 (1999).
[23] M. Pérez-Armendariz, C. Roy, D. C. Spray, and M. Bennett, Biophys. J. **59**, 76 (1991).
[24] M. A. Ravier, M. Güldenagel, A. Charollais, A. Gjinovci, D. Caille, G. Söhl, C. B. Wollheim, K. Willecke, J.-C. Henquin, and P. Meda, Diabetes **54**, 1798 (2005).
[25] P. Klee, F. Allagnat, H. Pontes, M. Cederroth, A. Charollais, D. Caille, A. Britan, J.-A. Haefliger, and P. Meda, J. Clin. Invest. **121**, 4870 (2011).
[26] P. Meda, Diabetes **61**, 1656 (2012).
[27] A. Loppini, A. Capolupo, C. Cherubini, A. Gizzi, M. Bertolaso, S. Filippi, and G. Vitiello, Phys. Lett. A **378**, 3210 (2014).
[28] C. Cherubini, S. Filippi, A. Gizzi, and A. Loppini, Phys. Rev. E **92**, 042702 (2015).
[29] A. Loppini, M. Braun, S. Filippi, and M. G. Pedersen, Phys. Biol. **12**, 066002 (2015).
[30] A. Loppini, M. G. Pedersen, M. Braun, and S. Filippi, Phys. Rev. E **96**, 032403 (2017).
[31] M. Scheffer, J. Bascompte, W. A. Brock, V. Brovkin, S. R. Carpenter, V. Dakos, H. Held, E. H. Van Nes, M. Rietkerk, and G. Sugihara, Nature (London) **461**, 53 (2009).
[32] M. Scheffer, S. R. Carpenter, T. M. Lenton, J. Bascompte, W. Brock, V. Dakos, J. Van de Koppel, I. A. Van de Leemput, S. A. Levin, E. H. Van Nes *et al.*, Science **338**, 344 (2012).
[33] V. Dakos, M. Scheffer, E. H. van Nes, V. Brovkin, V. Petoukhov, and H. Held, Proc. Natl. Acad. Sci. USA **105**, 14308 (2008).
[34] I. A. van de Leemput, M. Wichers, A. O. Cramer, D. Borsboom, F. Tuerlinckx, P. Kuppens, E. H. van Nes, W. Viechtbauer, E. J. Giltay, S. H. Aggen *et al.*, Proc. Natl. Acad. Sci. USA **111**, 87 (2014).
[35] V. Dakos and J. Bascompte, Proc. Natl. Acad. Sci. USA **111**, 17546 (2014).
[36] J. L. Payne, P. S. Dodds, and M. J. Eppstein, Phys. Rev. E **80**, 026125 (2009).
[37] X.-Z. Wu, P. G. Fennell, A. G. Percus, and K. Lerman, Phys. Rev. E **98**, 022321 (2018).